




Nonlocal and nonadiabatic Pauli potential for time-dependent orbital-free density functional theoryKaili Jiang (姜凯立) ^{1,*}, Xuecheng Shao (邵学成) ^{1,†} and Michele Pavanello ^{1,2,‡}¹*Department of Chemistry, 73 Warren St., Rutgers University, Newark, New Jersey 07102, USA*²*Department of Physics, 101 Warren St., Rutgers University, Newark, New Jersey 07102, USA*

(Received 9 September 2021; revised 10 November 2021; accepted 18 November 2021; published 6 December 2021)

Time-dependent orbital-free density functional theory is an efficient *ab initio* method for calculating the electronic dynamics of large systems. In comparison to standard time-dependent density functional theory, it computes only a single electronic state regardless of system size, but it requires an additional time-dependent Pauli potential term. We propose a nonadiabatic and nonlocal Pauli potential whose main ingredients are the time-dependent particle and current densities. Our calculations of the optical spectra of metallic and semiconductor clusters indicate that nonlocal and nonadiabatic time-dependent orbital-free density functional theory performs accurately for metallic systems and semiquantitatively for semiconductors. This paper opens the door to wide applicability of time-dependent orbital-free density functional theory for nonequilibrium electron and electron-nuclear dynamics of complex materials.

DOI: [10.1103/PhysRevB.104.235110](https://doi.org/10.1103/PhysRevB.104.235110)**I. INTRODUCTION**

The *ab initio* simulation of nanoscale quantum systems when their electrons are out of equilibrium is a challenging task [1–5], not only for time-dependent density functional theory (TD-DFT) but for almost all other electronic structure methods. One of the challenges is the computational cost involved in the simulations, which compounds on top of the already challenging computation of the ground state. In DFT and TD-DFT, the computational expense typically scales cubically with system size, and for wave-function-based methods the cost is even higher [6]. The *ab initio* methods currently available are thus not suited to address systems relevant to most experiments (where typical sizes of, for example, nanoclusters are in the range of 1 to 1000 nm [7–9]). Clearly, alternative methods are needed. Several research groups are actively working to tackle this issue by developing such methods as the semiempirical time-dependent density functional tight binding (TD-DFTB) [10], the simplified TD-DFT [11], and other methods more loosely rooted in quantum mechanics [12–17]. In this paper, we further the time-dependent orbital-free density functional theory (TD-OFDFT), an *ab initio* method with potentially far reduced computational cost compared to TD-DFT and even TD-DFTB.

TD-OFDFT tackles the scaling problem by only considering a single active orbital. In contrast, TD-DFT uses a number of orbitals equal to the number of electrons in the system. Thus, TD-OFDFT can achieve a linear computational scaling with the number of electrons so long as approximate functionals are used. In addition to the time-dependent exchange-correlation (XC) potential that also needs to be

approximated in TD-DFT [18], TD-OFDFT requires us to approximate the time-dependent Pauli potential [19–23]. Thus, the main challenge is to find a good approximation to this potential.

Early adoptions of TD-OFDFT utilize adiabatic and local density approximations, i.e., the adiabatic Thomas-Fermi [24,25] potential as the time-dependent Pauli potential, sometimes referred to as time-dependent Thomas-Fermi [26–28] or hydrodynamic DFT [29–32]. Such a simple approximation has been successful for systems such as Na clusters [27] but only qualitatively captures the spectra for other types of systems [29,33,34]. As we will show in this paper, for TD-OFDFT to be semiquantitative for a wide class of systems, the approximate time-dependent Pauli potential must be nonlocal and nonadiabatic [35–38].

To account for nonlocality, several nonlocal kinetic energy density functionals have been developed for ground state OFDFT [39–41]. These can be employed in TD-OFDFT by applying the so-called adiabatic approximation (i.e., the potentials are given by their ground-state expressions evaluated at the time-dependent electron density). To account for nonadiabaticity (i.e., going beyond the adiabatic approximation), potentials need to depend on the time-dependent electron density and at least the current density [18,20,42,43]. Along these lines of research, in this paper we derive an improved nonadiabatic correction to the time-dependent Pauli potential from a frequency-dependent Pauli kernel derived from the response of the free electron gas which we recently proposed [19].

Another challenge for TD-OFDFT has been the general lack of software that implements it. We recently filled this gap by developing DFTPY [34], an object-oriented PYTHON software for OFDFT as well as real-time and linear-response (Casida [44]) TD-OFDFT. DFTPY is fully parallelized using MPI4PY [45], and scales well with system size as we showed in Ref. [34].

*kaili.jiang@rutgers.edu

†xs161@newark.rutgers.edu

‡m.pavanello@rutgers.edu

This paper is structured as follows. In Sec. II, we briefly introduce the formalism of TD-OFDFT and derive the proposed nonadiabatic correction to the time-dependent Pauli potential from the frequency-dependent Pauli kernel. Section III lays out the computational details. In Sec. IV we present the optical spectra derived from real-time TD-OFDFT simulations carried out in a linear-response regime (weak perturbation) of several representative metallic and semiconductor systems. And, finally, in the Appendix, we discuss the implementation of the nonadiabatic Pauli potential in DFTPY.

II. FORMALISM

A. Time-dependent Schrödinger-like equation for TD-OFDFT

In this section, we provide a brief introduction to the formalism behind TD-OFDFT. For more details, we refer the readers to Refs. [19,20,46]. In TD-OFDFT, one-to-one invertible maps are established between the real system of interacting electrons, the fictitious system of noninteracting electrons (aka the KS system), and a fictitious system of noninteracting bosons. The bosonic system yields the following density-wave-function relationship:

$$n(\mathbf{r}, t) = N|\phi_B(\mathbf{r}, t)|^2, \quad (1)$$

where $\phi_B(\mathbf{r}, t)$ is a normalized bosonic wave function, N is the number of electrons in the system. Throughout, the subscription B stands for bosonic system.

In this paper, we only consider systems at zero temperature. In a typical setup for real-time propagations, the system starts with its ground-state density $n_0(\mathbf{r})$ and at $t = 0$ the system is perturbed out of equilibrium. A time-dependent Schrödinger-like equation is employed to propagate the system for $t > t_0$ (atomic units are used throughout this paper):

$$\left[-\frac{\nabla^2}{2} + v_B[n](\mathbf{r}, t) \right] \phi_B(\mathbf{r}, t) = i \frac{\partial}{\partial t} \phi_B(\mathbf{r}, t). \quad (2)$$

When optical spectra are sought, the typical initial condition is

$$\phi_B(\mathbf{r}, t_0) = \frac{1}{\sqrt{N}} \sqrt{n_0(\mathbf{r})} e^{i\mathbf{k}\cdot\mathbf{r}}, \quad (3)$$

where the exponential term $e^{i\mathbf{k}\cdot\mathbf{r}}$ effectively donates momentum of strength $k = |\mathbf{k}|$ along the direction of vector \mathbf{k} to the electronic system as the initial, weak perturbation [47].

The time-dependent effective potential is given by

$$v_B[n](\mathbf{r}, t) = v_F[n](\mathbf{r}, t) + v_S[n](\mathbf{r}, t), \quad (4)$$

where $v_F[n](\mathbf{r}, t)$ is the time-dependent Pauli potential, which is the difference between the bosonic noninteracting kinetic potential and the fermionic one, and $v_S[n](\mathbf{r}, t)$ is the time-dependent KS potential. Such a decomposition of the effective potential acting on the bosonic system is borrowed from the ground-state decomposition of the noninteracting kinetic energy, $T_S[n]$, namely,

$$T_S[n] = T_{vw}[n] + T_F[n], \quad (5)$$

where $T_{vw}[n]$ is the von Weizsäcker kinetic energy (i.e., the kinetic energy of a set of noninteracting bosons in their ground state) and $T_F[n]$ is the Pauli kinetic energy. It is said that the

Pauli potential introduces the effects of the Pauli exclusion principle in the bosonic electronic structure of Eq. (2).

The corresponding adiabatic approximation for the Pauli potential is given by the functional derivative of the Pauli energy evaluated at the time-dependent electron density, namely,

$$v_p^{\text{ad}}(\mathbf{r}, t) = \left. \frac{\delta T_F[n_0]}{\delta n_0(\mathbf{r})} \right|_{n_0(\mathbf{r}) \rightarrow n(\mathbf{r}, t)}. \quad (6)$$

However, to achieve accurate results in TD-OFDFT, the nonadiabatic contribution to the potential should not be neglected. Therefore, the total Pauli potential can be represented as the adiabatic portion plus a nonadiabatic correction:

$$v_p(\mathbf{r}, t) = v_p^{\text{ad}}(\mathbf{r}, t) + v_p^{\text{nad}}(\mathbf{r}, t). \quad (7)$$

The nonadiabatic contribution to the Pauli potential has much stronger effects on the electron dynamics compared to the nonadiabatic contribution to the XC potential [18]. The latter needs to bridge the dynamics of N noninteracting electrons with the one of N interacting electrons. Thus, states described by so-called double excitations and beyond need to be accounted for by the nonadiabatic XC term. In contrast, the nonadiabatic contribution to the Pauli potential needs to bridge the dynamics of N noninteracting bosonic electrons to the one of N noninteracting fermionic electrons, therefore it needs to create all those excitations that are missing when exciting a single effective electron in comparison to exciting N fermionic electrons. We expect the nonadiabaticity in the Pauli potential to be very strong and to account for qualitative aspects of the electronic response. This, in fact, was the essence of our recent work [19] which focused on the first excited state of selected systems.

B. Approximating the nonadiabatic Pauli potential

In this section, we will derive a nonadiabatic correction to the Pauli potential from a nonadiabatic Pauli kernel developed by us previously [19]. In that study, we derived a Pauli kernel relying on the Dyson equation connecting the bosonic response, χ_B , with the Kohn-Sham response, χ_S ,

$$\chi_B^{-1}(\mathbf{r}, \mathbf{r}', \omega) - \chi_S^{-1}(\mathbf{r}, \mathbf{r}', \omega) = f_p(\mathbf{r}, \mathbf{r}', \omega). \quad (8)$$

By substituting in Eq. (8), the frequency-dependent Lindhard function for χ_S and the response of a free boson gas for χ_B , one obtains an expression for f_p which can be expanded in terms of unitless variables, $\bar{\eta} = \frac{q}{2k_F}$, $\bar{\omega} = \frac{\omega}{qk_F}$, $\bar{\gamma} = \frac{\eta}{qk_F}$, where q is the conjugate variable to $|\mathbf{r} - \mathbf{r}'|$, ω is the frequency of the external time-dependent perturbation, and η is the broadening parameter introduced to implement causality [48].

Retaining terms up to the first order of ω and discarding the adiabatic part which is frequency independent,

$$f_p^{\text{nad}}(\mathbf{r}, q, \omega) = \frac{i\pi^3}{12} \left(\frac{6}{k_F^2(\mathbf{r})q} + \frac{q}{k_F^4(\mathbf{r})} \right) \omega, \quad (9)$$

where the local density approximation for the Fermi wave vector is introduced, $k_F(\mathbf{r}) = (3\pi^2 n(\mathbf{r}))^{1/3}$.

We now use the nonadiabatic Pauli kernel to approximate the nonadiabatic correction to the time-dependent Pauli potential adopting the same technique as described in Ref. [20].

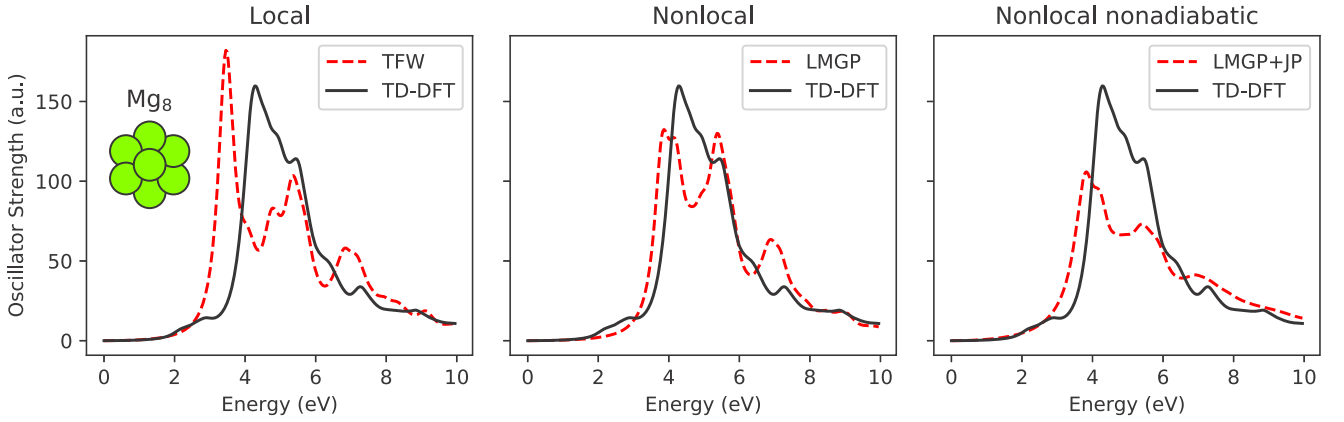


FIG. 1. Optical spectrum of the Mg_8 cluster (see inset for a snapshot of the structure). LMGP is a nonlocal kinetic energy functional with density dependent kernel [41] employed in the adiabatic approximation (i.e., $v_p(t) \simeq v_p[n_0 = n(t)]$). LMGP + JP stands for adiabatic LMGP augmented by the additional propagation step with the nonadiabatic potential in Eq. (15).

Considering the continuity equation

$$\frac{\partial n(\mathbf{r}', t)}{\partial t} = -\nabla \cdot \mathbf{j}(\mathbf{r}', t), \quad (10)$$

and expanding the density at t' around time t up to the first order, we obtain

$$\begin{aligned} \delta n(\mathbf{r}', t') &\approx \delta n(\mathbf{r}', t) + \frac{\partial n(\mathbf{r}', t)}{\partial t}(t - t') \\ &= \delta n(\mathbf{r}', t) - \nabla \cdot \mathbf{j}(\mathbf{r}', t)(t - t'). \end{aligned} \quad (11)$$

Using the definition of the Pauli kernel,

$$f_p(\mathbf{r}, \mathbf{r}', t - t') = \frac{\delta v_p(\mathbf{r}, t)}{\delta n(\mathbf{r}', t')}, \quad (12)$$

we can write the variation of the Pauli potential as

$$\delta v_p(\mathbf{r}, t) = \int d\mathbf{r}' \int d(t - t') \delta n(\mathbf{r}', t') f_p(\mathbf{r}, \mathbf{r}', t - t'). \quad (13)$$

When plugging Eq. (11) into Eq. (13), we note that the $\delta n(\mathbf{r}', t)$ term in Eq. (11) only depends on the density at time t and therefore yields the adiabatic part of the Pauli potential. From the second term of Eq. (11), we derive the nonadiabatic part of the Pauli potential,

$$\begin{aligned} v_p^{\text{nad}}(\mathbf{r}, t) &= - \int d\mathbf{r}' \nabla \cdot \mathbf{j}(\mathbf{r}', t) \int d(t - t')(t - t') f_p(\mathbf{r}, \mathbf{r}', t - t') \\ &= - \int d\mathbf{r}' \nabla \cdot \mathbf{j}(\mathbf{r}', t) \frac{-i \partial f_p(\mathbf{r}, \mathbf{r}', \omega)}{\partial \omega} \\ &= - \mathcal{F}^{-1} \left\{ i \mathbf{q} \cdot \mathbf{j}(\mathbf{q}, t) \frac{-i \partial f_p(\mathbf{q}, \omega)}{\partial \omega} \right\}, \end{aligned} \quad (14)$$

where $\mathcal{F}^{-1}\{\cdot\}$ represents inverse Fourier transform in the space domain.

We immediately clarify that Eq. (14) is approximate—not only because the time-dependent density is expanded only to first order but, most importantly, because the recovered quantity is not v_p^{nad} but its first-order variation δv_p^{nad} . Formally, a procedure of functional integration should be employed

which, unlike the static case [40,49,50], is not straightforward in the time domain.

Finally, we plug Eq. (9) into Eq. (14) and note that the derivative of the adiabatic contribution of f_p with respect to ω vanishes; we obtain

$$\begin{aligned} v_p^{\text{nad}}(\mathbf{r}, t) &= - \frac{\pi^3}{12} \left(\frac{6}{k_F^2(\mathbf{r})} \mathcal{F}^{-1} \left\{ i \mathbf{q} \cdot \mathbf{j}(\mathbf{q}, t) \frac{1}{q} \right\} \right. \\ &\quad \left. + \frac{1}{k_F^4(\mathbf{r})} \mathcal{F}^{-1} \{ i \mathbf{q} \cdot \mathbf{j}(\mathbf{q}, t) q \} \right). \end{aligned} \quad (15)$$

We note that Eq. (15) corrects the potential proposed by White *et al.* [20] with the addition of a second term. As our calculations will demonstrate, the second term of Eq. (15) is key to achieving accurate results and thus should not be neglected.

III. COMPUTATIONAL DETAILS

The TD-OFDFT calculations are performed with DFTPY [34] and the benchmark TD-DFT calculations are performed with embedded QUANTUM ESPRESSO's TD-DFT implementation [51–53]. All TD-OFDFT and TD-DFT calculations employ the same adiabatic Perdew-Zunger local density approximation (LDA) [54] as the XC functional and OEPP [55] pseudopotentials unless otherwise stated. The kinetic energy cutoff for the TD-DFT wave functions and the TD-OFDFT density are chosen to converge the ground-state energy within 1 meV/atom. The oscillator strength is calculated using $\sigma(\omega) = -\omega \text{Im}[\frac{\delta \tilde{\mu}(\omega)}{k}]$, where $\delta \tilde{\mu}(\omega)$ is the Fourier transform of the dipole moment change calculated at every time step of the propagation and k is the kick strength mentioned in Eq. (3). The kick strength $k = 1.0 \times 10^{-3}$ a.u. is used for all calculations. The time step chosen is consistent with the plane-wave cutoff employed and is $dt = 0.1$ a.u. in all simulations, except for Ag, Si, and GaAs simulations with the Local-kF Mi-Genova-Pavanello (LMGP) functional, where the time step is $dt = 0.01$ a.u.

IV. RESULTS AND DISCUSSION

To test the regime of applicability of TD-OFDFT, we must carry out proof of principle simulations on an array of possible

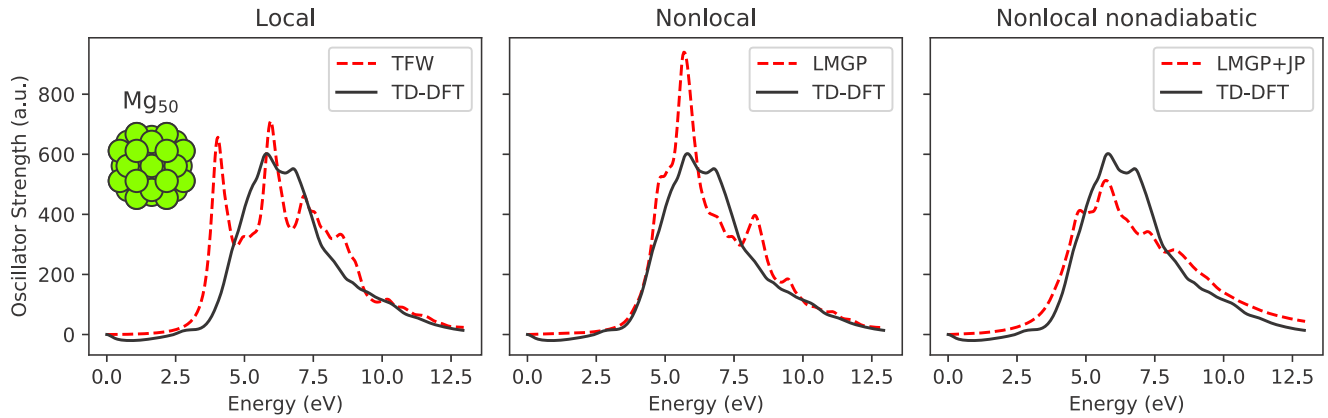


FIG. 2. Optical spectrum of the Mg_{50} cluster. See caption to Fig. 1 for additional details.

electronic structures. For sake of simplicity, in this paper we target the optical spectrum as observable and we focus on clusters from small sizes (eight atoms) to medium sizes (up to about 300 atoms). The ability to predict optical spectra tests how well the electronic-structure method reproduces the linear response function of the electronic system, and with that it probes the energy levels and transition dipole moments. The most appropriate benchmark is standard TD-DFT—a method that employs the exact Pauli potential. Therefore, any deviation in the shape of the spectral envelope or the peak positions from TD-DFT are directly ascribed to the errors introduced by the approximate Pauli potential employed in TD-OFDFT.

For this test, we choose clusters of three metallic systems (Mg, Na, Ag) and two semiconductors (Si, GaAs). We have previously showed that nonlocal OFDFT is able to reproduce well the electronic structure of these systems in their ground state [41]. However, functionals that behave well for ground states may not provide an equally accurate description when going to the time domain—the reason being the need in practical calculations to involve the adiabatic approximation when evaluating the density-dependent potentials.

In all figures presented in this section, we indicate by LMGP the inclusion of adiabatic nonlocal Pauli potential by simply evaluating the optical spectra with the nonlocal LMGP kinetic energy functional using the adiabatic approximation [i.e., at every time t we evaluate its potential at the time-

dependent density, $n(\mathbf{r}, t)$, as shown in Eq. (6)]. LMGP + JP instead, indicates that in addition to LMGP we add the nonadiabatic contribution derived in Eq. (15).

A. Metallic systems

Previously [34], we investigated the TD-OFDFT optical spectra of Mg clusters with the adiabatic Thomas-Fermi approximation for the Pauli potential (TFW here onward). Our results showed that TFW could approach the TD-DFT result only qualitatively. Figure 1 shows that TD-OFDFT can reach quantitative agreement with TD-DFT provided nonlocality (with the LMGP kinetic energy functional) and nonadiabaticity (adding to LMGP the nonadiabatic contributions to the Pauli potential) are included.

The effect on the optical spectrum of Mg_8 of including nonlocality in the Pauli potential is very strong. TFW significantly redshifts the first absorption band compared to the benchmark TD-DFT results. Accounting for nonlocality in the Pauli potential brings the spectrum much closer to the TD-DFT benchmark. However, the spectral envelope is not recovered fully. When the nonadiabatic correction is included, then TD-OFDFT recovers the TD-DFT spectral envelope despite slightly increasing the spectral weights in the tail of the spectrum at high energies, depleting of intensity the main spectral features.

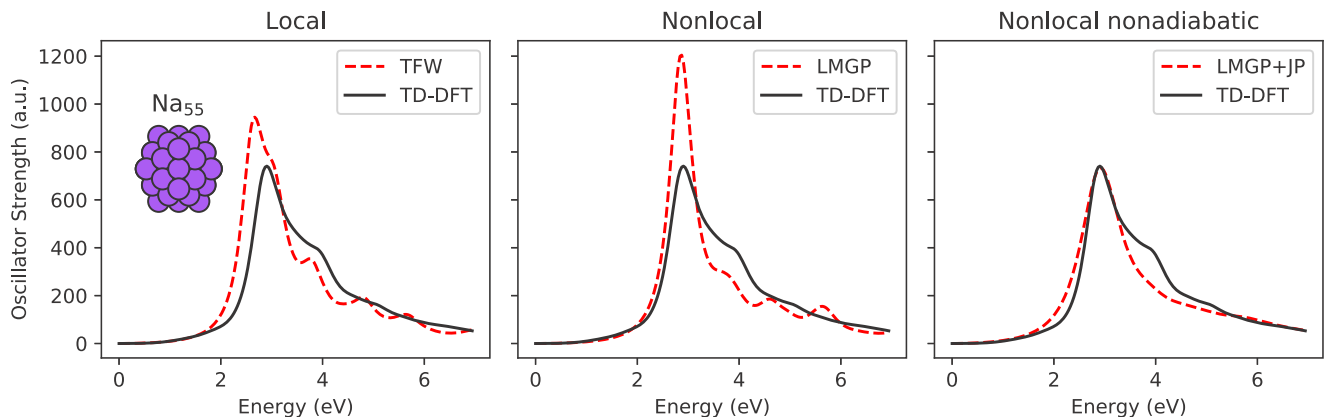


FIG. 3. Optical spectrum of the Na_{55} cluster. See caption to Fig. 1 for additional details.

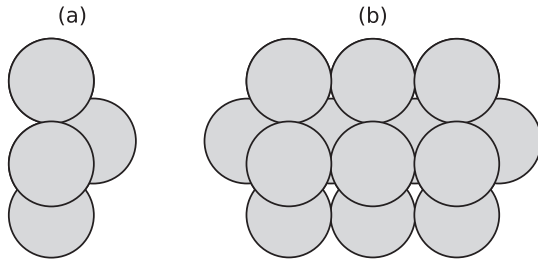


FIG. 4. (a) Ag_n nanorod building block. (b) $n = 19$ nanorod. The procedure for building the Ag nanorods is taken from Refs. [56,57].

In Fig. 2, we report the computed optical spectrum of a Mg_{50} cluster. The inclusion of nonlocality and nonadiabaticity in the Pauli potential has very similar effects in the spectrum to that of the Mg_8 cluster, with the nonlocal term shifting the peaks to the correct position and the nonadiabatic term adjusting the shape of the spectral envelope. It is also worth noting that the TD-OFDFT results get more accurate as the systems grow larger in size because the larger the system the more likely it is to develop free-electron-gas-like electronic structure in its core [34].

We now shift to Na clusters. In all past investigations, even the simplest of approximations for the Pauli potential (i.e., TFW) resulted in oscillator strengths that agree well with the TD-DFT result [27]. In light of the simulations presented here, it is clear that such agreement is largely due to error cancellation between the missing adiabatic nonlocal term and nonadiabatic correction in TFW. In this paper, we take a look at an icosahedron Na cluster containing 55 Na atoms, see Fig. 3.

We therefore expect that the spectrum calculated with TFW matches well with the TD-DFT benchmark with only a slight redshift, confirming previous results [27]. When accounting for the nonlocal correction to the adiabatic Pauli potential computed at the LMGP level, peaks shift to the correct position but the strength of the main peak at ~ 3 eV is overestimated. Only after including both nonlocal and nonadiabatic corrections does TD-OFDFT yield a spectral envelope that is very close to the one from TD-DFT. Thus, it is clear that error cancellation is a big player in the previously reported good results from the TFW approximation for the Pauli potential.

TABLE I. Comparison of the excitation energy of the longitudinal plasmon peaks of Ag rods of increasing length. TD-DFT and TD-DFTB are taken from Ref. [56]. The shorthand notations pos and shift stand for peak position (excitation energy) and shift from the Ag_{19} system, respectively. Energy units are eV.

System	TD-DFT		TD-DFTB		TFW		LMGP+JP	
	pos	shift	pos	shift	pos	shift	pos	shift
Ag_{19}	3.56		2.67		2.50		2.66	
Ag_{25}	3.27	-0.29	2.58	-0.09	2.39	-0.11	2.51	-0.15
Ag_{31}	3.01	-0.55	2.41	-0.26	2.26	-0.24	2.36	-0.30
Ag_{37}	2.77	-0.79	2.26	-0.41	2.15	-0.35	2.22	-0.44
Ag_{43}	2.57	-0.99	2.08	-0.59	2.05	-0.45	2.11	-0.55
Ag_{49}	2.41	-1.15	2.02	-0.65	1.95	-0.55	2.01	-0.65
Ag_{55}	2.30	-1.26	1.91	-0.76	1.85	-0.65	1.91	-0.75
Ag_{61}	2.04	-1.52	1.74	-0.93	1.71	-0.79	1.76	-0.90

Silver is an important transition metal with high applicability to chemistry and engineering. Thus, its electronic response has often been the subject of approximate models [55,56]. We compute the longitudinal plasmon excitation of Ag nanorods and compare against TD-DFT and the semiempirical TD-DFTB presented in Ref. [56]. Snapshots of the Ag nanorods used can be found in Fig. 4.

Even though the TD-DFT and TD-DFTB calculations were carried out with the Perdew-Burke-Ernzerhof XC functional and the DZ basis set [56], which differ from the setup of our TD-OFDFT calculations (we employ LDA XC and plane waves), the trends in the computed excitation energies should not be strongly dependent on the choice of local or semilocal XC functionals [58]. Table I shows that TD-OFDFT with TFW is very close to the TD-DFTB result and LMGP + JP is essentially on top of TD-DFTB. In inspecting the table, we see that TD-OFDFT correctly captures the trend that the peaks shift to the red as the Ag rod's length increases. However, one wonders why the TFW approximation (which is both adiabatic and local) does so well in comparison to the nonadiabatic and nonlocal calculation. Clearly, the answer must be error cancellation. We have witnessed error cancellation before for Na clusters (see Fig. 3) where TFW delivered results almost as good as LMGP + JP. It is possible that, similarly to the Na clusters, the longitudinal plasmon mode for the Ag rods

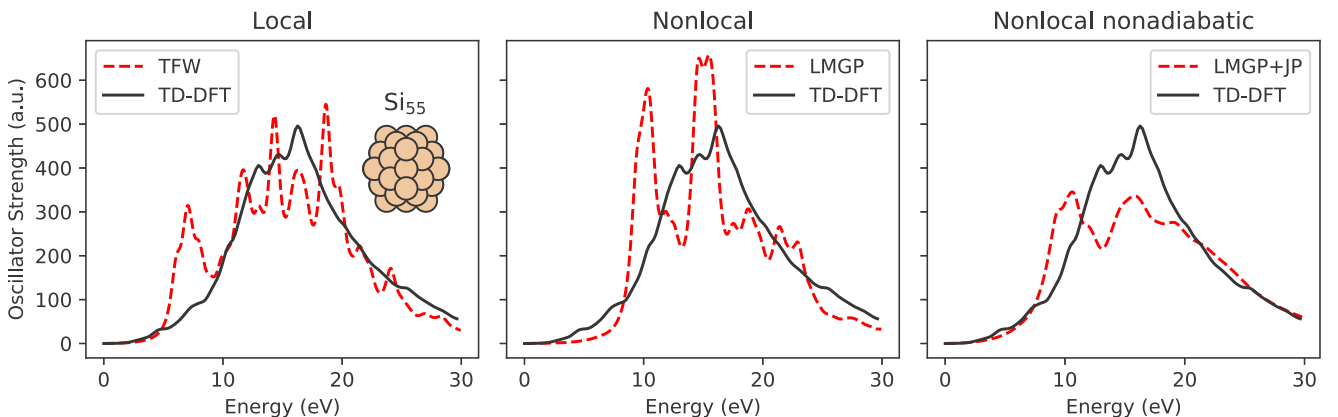


FIG. 5. Optical spectrum of the Si_{55} cluster. See caption to Fig. 1 for additional details.

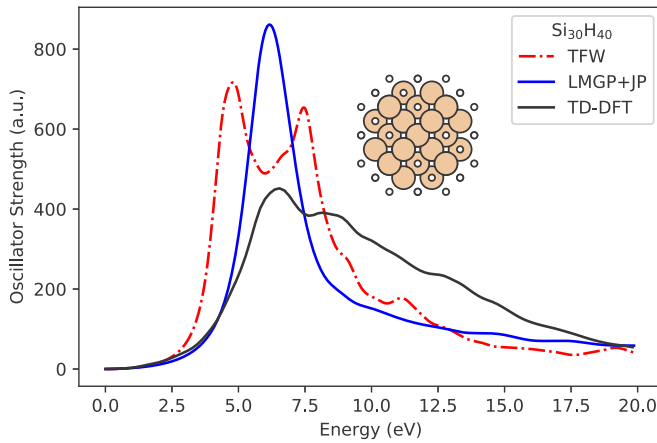


FIG. 6. Optical spectrum of the $\text{Si}_{30}\text{H}_{40}$ cluster (see picture in the inset for the structure of the cluster). Solid black: TD-DFT benchmark. Dash-dotted red: TFW (local). Solid blue: LMGP + JP (nonlocal and nonadiabatic).

behaves similarly to a free electron gas—dynamics which is already captured by the TFW functional in the adiabatic approximation.

B. Semiconductor systems

We start the investigation of the optical spectra of clusters of semiconducting systems with a Si_{55} icosahedral cluster carved in a way analogous to the metallic clusters mentioned in the previous section, see Fig. 5. TFW and LMGP only qualitatively capture the spectra, with several peaks with overestimated oscillator strength. For LMGP, the peaks at ~ 10 eV and ~ 15 eV are too strong. The nonadiabatic correction to the Pauli potential recovers the correct spectral envelope by lowering the oscillator strengths of these two peaks in favor of an increased intensity in the high-energy tail of the spectrum.

Broadening of the energy levels results from the fact that the fermionic system has a higher density of states compared

to the bosonic system. The increase of the number of excited states leading to broadening is an important feature of the nonadiabatic correction to the Pauli potential.

We move on to consider an additional silicon system, Si_{30} cluster cut from a crystal diamond Si bulk structure. We also consider the H-passivated version of the cluster employing the passivation protocol described elsewhere [59] (i.e., for each dangling Si bond, we put a hydrogen atom on the other end of the bond). We carefully chose the size of the structure so each Si atom can have at most two Si-H bonds. In contrast to the icosahedron clusters which are more metallic, this configuration of the Si cluster is more semiconductorlike. The optical spectrum for this system is available in Fig. 6. TFW does not yield the correct peak position in the spectrum. Instead, LMGP + JP obtains the correct position of the lowest-lying peak while it blends away the other features of the spectrum.

To interrogate TD-OFDFT's ability to predict trends when chemical changes are applied to the system, in Fig. 7 we compare the effect of passivation on the optical spectrum. TD-DFT predicts that the passivation induces a slight redshift of the spectrum. Interestingly, a similar redshift can also be observed in the LMGP + JP TD-OFDFT result.

OFDFT can perform well for III-V semiconductors [39–41,60]. Figure 8 compares the optical spectrum computed with TD-OFDFT and TD-DFT for a Ga_4As_4 cluster. Once again, by accounting for nonlocality and nonadiabaticity in the Pauli potential, the TD-OFDFT spectra are very similar to the TD-DFT benchmark result.

C. Going beyond the capabilities of TD-DFT

The optical spectrum of large nanoparticles is an important experimental characterization for optoelectronic materials [61]. In this section, we consider a $\text{Ga}_{152}\text{As}_{152}$ nanoparticle cut from the bulk GaAs structure and passivated in a similar way as described previously for Si. Following a well-established recipe [59], for GaAs quantum dots instead of passivating with H atoms, for each Ga atom a pseudo H atom

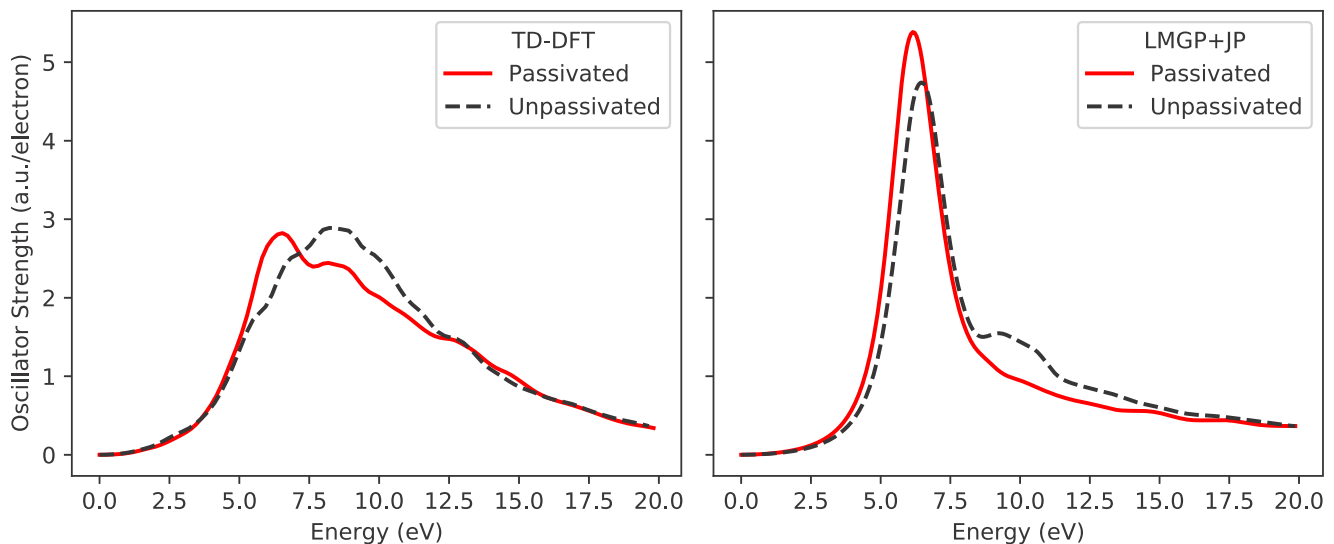


FIG. 7. Effects of passivation with H atoms on the optical spectrum of Si_{30} . Left panel: TD-DFT. Right panel: TD-OFDFT carried out with with adiabatic LMGP plus nonadiabatic correction (LMGP + JP).

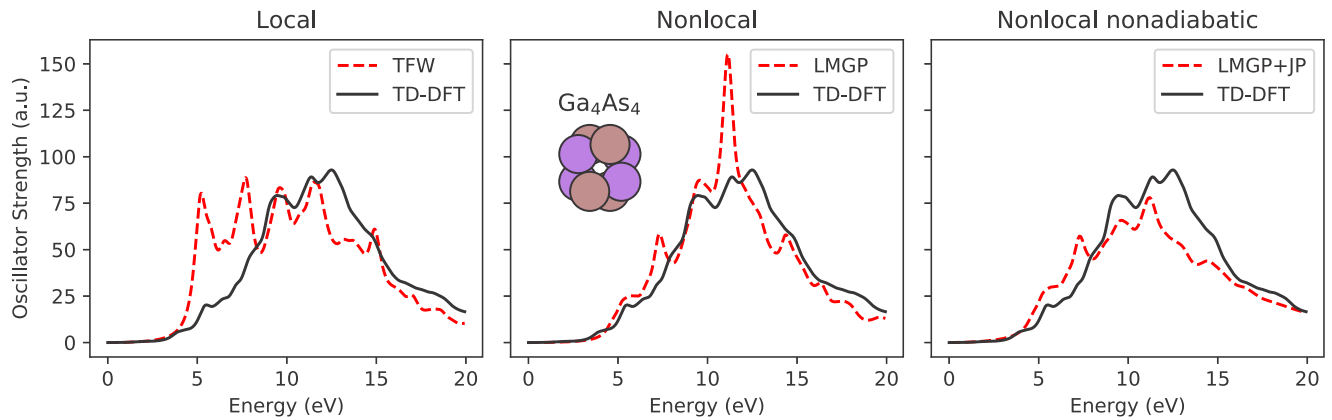


FIG. 8. Optical spectrum of the Ga_4As_4 cluster. See caption to Fig. 1 for additional details.

with 1.25 electrons and for each As atom a pseudo H atom with 0.75 electrons are used.

Tackling this system with TD-DFT would be a major undertaking probably requiring specialized software and high performance computing hardware. Our TD-OFDFT method only required a single compute node (36 cores). Conceivably, with available high-performance computing, TD-OFDFT would be able to approach much larger system sizes compared to TD-DFT as we have showcased for ground states in a previous work [62] where complex materials could be approached with nonlocal kinetic energy functionals. To provide further context, we mention here that in another prior work [34] we showed that DFTPY with nonlocal functionals achieves linear computational scaling up to system sizes of 1 000 000 atoms.

Figure 9 illustrates the optical spectrum for the passivated and unpassivated nanoparticles computed with the nonlocal and nonadiabatic method LMGP + JP in comparison with

experimental spectra recorded for bulk and nanoparticle GaAs systems.

Interestingly, TD-OFDFT recovers the main spectral feature at ~ 5 eV as well as the smaller feature at ~ 6 eV for both the bulk and nanoparticle systems.

It is important to note that TD-OFDFT misses the band-gap transition at ~ 2.5 eV, which is prominent in the spectrum of bulk GaAs. Because OFDFT does not have a notion of single-particle orbitals or bands, it is not surprising that several details in the optical spectra related to interband transitions are missing in TD-OFDFT. Formally, these would be recovered by the nonadiabatic Pauli potential. However, in this paper, we have developed a nonadiabatic potential derived from the free electron gas. Thus, it would simply be too much to ask from the free electron gas to also be able to reproduce interband transitions in GaAs. Overall, despite the mentioned flaws, the agreement between the TD-OFDFT and the experiment is better than semiquantitative.

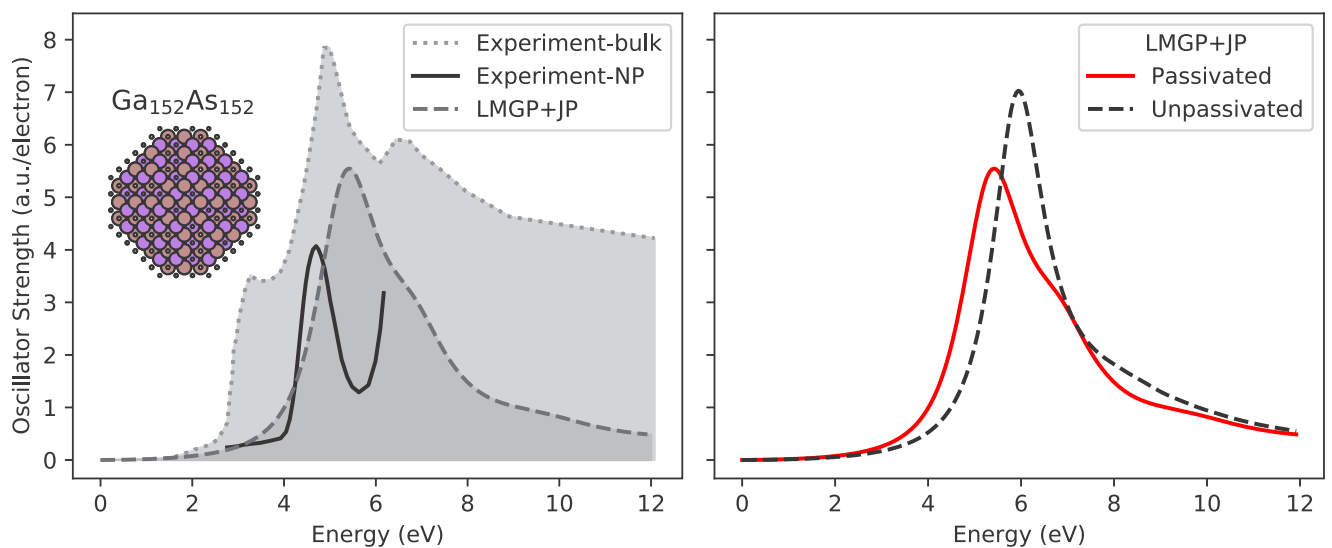


FIG. 9. Left: TD-OFDFT optical spectrum of a passivated $\text{Ga}_{152}\text{As}_{152}$ nanoparticle carried out with adiabatic LMGP plus nonadiabatic correction (LMGP + JP). Experimental spectrum for GaAs nanoparticles (experiment-NP) is taken from Ref. [63] and is noticeably of lower overall resolution compared to the spectrum of bulk GaAs which is taken from Ref. [64]. Right: Effects of passivation on the optical spectrum of the nanoparticle predicted with TD-OFDFT.

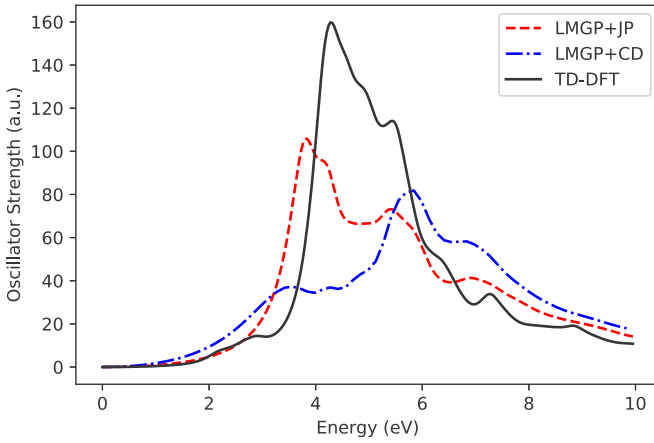


FIG. 10. Optical spectrum of the Mg_8 cluster (same as in Fig. 1) computed with TD-DFT and two versions of the nonadiabatic Pauli potential (see text for details).

D. Comparison against a truncated nonadiabatic Pauli potential

As mentioned, in Ref. [20] the authors pioneered the use of a nonadiabatic Pauli potential in real-time TD-OFDFT simulations. Their so-called current-dependent potential reads as follows [see Eq.(15) of the reference]:

$$v_p^{\text{CD}}(\mathbf{r}, t) = \frac{\pi^3}{2k_F^2(\mathbf{r})} \mathcal{F}^{-1} \left\{ i\mathbf{q} \cdot \mathbf{j}(\mathbf{q}, t) \frac{1}{q} \right\}, \quad (16)$$

which can be identified as the first term of Eq. (15). Here we wish to determine the effect of neglecting the second term on the optical spectra. The physical picture is that Eq. (16) handles the low- q dependence of the potential in the same way the Thomas-Fermi functional handles the low- q density dependence of the kinetic energy functional. The second term of Eq. (15), instead, behaves in a way reminiscent of the von Weizsäcker term (i.e., it goes like q^2). Therefore, in systems where large q values are sampled (such as in clusters and any nonperiodic system), we expect the second term to play a significant role.

In Fig. 10, we report the optical spectra of Mg_8 computed with TD-DFT and nonadiabatic TD-OFDFT with the two options for the nonadiabatic potential [LMGP + JP corresponds to Eq. (15), LMGP + CD corresponds to Eq. (16)]. From the figure, it is clear that the von Weizsäcker-like term is instrumental in achieving semiquantitative agreement with the TD-DFT reference calculation. Once again, we believe the reason stems from the recovered q^2 behavior of the additional term present in Eq. (15).

V. CONCLUSION

We proposed and implemented a nonadiabatic (current-dependent) Pauli potential for time-dependent orbital-free DFT, TD-OFDFT, simulations of electron dynamics in materials. The nonadiabatic part of the Pauli potential is responsible for major qualitative features in the optical spectrum because it bridges the dynamics of N noninteracting bosons with the one of N noninteracting electrons. The proposed potential derives from the frequency-dependent dielectric function of the free electron gas.

We test our method on clusters of metallic elements (Na, Mg, Ag) and semiconductors (Si, GaAs). In most cases, we find TD-OFDFT to be close to benchmark TD-DFT spectra. TD-DFT is chosen as a benchmark because it relies on an exact description of the N -electron fermionic system (i.e., exact time-dependent Pauli potential). The study of Na clusters revealed that previous investigations bare of the nonadiabatic Pauli potential enjoyed strong error cancellation between the absence of nonadiabaticity in the potential and errors introduced in the adiabatic part of the potential (which we address employing the LMGP nonlocal kinetic energy functional).

In line with expectations, when studying semiconductors, TD-OFDFT struggles in the quantitative description of spectral features attributed to interband excitations. However, even for such difficult cases as GaAs nanoparticles, the method captures close to quantitatively the optical spectra and overall spectral envelopes.

An interesting future investigation would be to test the applicability of semilocal (GGA [60,65–68] and meta-GGA [69–72]) Pauli adiabatic potentials in place of the nonlocal ones tested in this work. This could result in important computational savings.

In sum, we developed an efficient method for the study of nonequilibrium electron dynamics of realistically sized materials setting the stage for using time-dependent orbital-free methods for simulating complex systems out of equilibrium for chemistry, energy applications, and beyond.

ACKNOWLEDGMENTS

This work is supported by the U.S. Department of Energy, Office of Basic Energy Sciences, under Award No. DE-SC0018343. The authors acknowledge the Office of Advanced Research Computing (OARC) at Rutgers, The State University of New Jersey for providing access to the Amarel and Calburn clusters and associated research computing resources that have contributed to the results reported here [73].

APPENDIX: IMPLEMENTATION OF THE NONADIABATIC POTENTIAL

We numerically solve Eq. (2) in the usual way by a propagation method implemented in our software package DFTPY. We choose the Crank-Nicolson propagator for this task, with a predictor-corrector up to any desired order. We refer the readers to Ref. [34] for the details of the implementation. In short, the propagator is to solve the following equation:

$$\left(1 + i\frac{dt}{2}\hat{H}\right)\phi_B(t+dt) = \left(1 - i\frac{dt}{2}\hat{H}\right)\phi_B(t). \quad (\text{A1})$$

Typically, the predictor-corrector only checks the density to be converged [74,75]. However, to implement a current-dependent potential such as the one in Eq. (15), the predictor-corrector needs to be modified to include the current density, i.e., $|j_{\text{corr}} - j_{\text{pred}}| < \epsilon$. Unfortunately, this often results in a large number of predictor-corrector loops, increasing computation time and causing numerical instabilities. To resolve this issue, we implemented the nonadiabatic potential as a correction with a separate Taylor-like propagation.

To achieve this goal, we first write the Hamiltonian as

$$\hat{H}(t) = \hat{H}^0(t) + \hat{H}'(t), \quad (\text{A2})$$

where \hat{H}' includes the nonadiabatic potential in Eq. (15) and \hat{H}^0 includes everything else. The solution of the time-dependent Schrödinger-like Eq. (2) can be expressed in terms of a time evolution operator [75]

$$\phi_B(t + dt) \approx \exp\left[-i\hat{H}\left(t + \frac{dt}{2}\right)dt\right]\phi_B(t), \quad (\text{A3})$$

where the approximation implies a small dt .

In the first step, we use the Crank-Nicolson propagator with a predictor-corrector for only $\hat{H}^0(t)$. We essentially obtain

$$\phi_B^0(t + dt) \approx \exp\left[-i\hat{H}^0\left(t + \frac{dt}{2}\right)dt\right]\phi_B(t). \quad (\text{A4})$$

Plug Eq. (A4) into Eq. (A3), we obtain

$$\phi_B(t + dt) \approx \exp\left[-i\hat{H}'\left(t + \frac{dt}{2}\right)dt\right]\phi_B^0(t + dt). \quad (\text{A5})$$

Note here we used the approximation $\exp[-i\hat{H}(t + \frac{dt}{2})dt] \approx \exp[-i\hat{H}^0(t + \frac{dt}{2})dt]\exp[-i\hat{H}'(t + \frac{dt}{2})dt]$. Even though \hat{H}' does not commute with \hat{H}^0 , the cross terms are in the second and higher orders of dt . In the case of small dt , the cross terms are negligible.

In the case of small $\hat{H}'(t)$ and small dt , we can make the assumption that $\hat{H}'(t + \frac{dt}{2}) \approx \hat{H}'(t)$ and Taylor expand Eq. (A5) up to the first order

$$\phi_B(t + dt) = [1 - i\hat{H}'(t)dt]\phi_B^0(t + dt). \quad (\text{A6})$$

Therefore, as the second step, we use the first-order Taylor propagator to propagate the nonadiabatic correction. We tested this method for a Mg_8 cluster and achieved a nearly identical result compared to propagating the whole Hamiltonian with the Crank-Nicolson propagator.

We note that when using Eq. (15) for clusters, the $k_F^{-4}(\mathbf{r})$ dependence of the second term can cause numerical instabilities in low-density regions. In such a case, a mask function such as $1 - 1/\{1 + [n(\mathbf{r})/n_{\text{cutoff}}]^2\}$ can be applied to the second term to fix the numerical instabilities.

-
- [1] J. Schirmer and A. Dreuw, Critique of the foundations of time-dependent density-functional theory, *Phys. Rev. A* **75**, 022513 (2007).
- [2] A. Holas, M. Cinal, and N. H. March, Comment on ‘‘Critique of the foundations of time-dependent density-functional theory,’’ *Phys. Rev. A* **78**, 016501 (2008).
- [3] N. T. Maitra, R. van Leeuwen, and K. Burke, Comment on ‘‘Critique of the foundations of time-dependent density-functional theory,’’ *Phys. Rev. A* **78**, 056501 (2008).
- [4] J. Schirmer and A. Dreuw, Reply to ‘‘Comment on ‘Critique of the foundations of time-dependent density-functional theory,’’’’ *Phys. Rev. A* **78**, 056502 (2008).
- [5] G. Vignale, Real-time resolution of the causality paradox of time-dependent density-functional theory, *Phys. Rev. A* **77**, 062511 (2008).
- [6] A. S. Pereira Gomes and C. R. Jacob, Quantum-chemical embedding methods for treating local electronic excitations in complex chemical systems, *Ann. Rep. C (Phys. Chem.)* **108**, 222 (2012).
- [7] E. Ringe, Shapes, plasmonic properties, and reactivity of magnesium nanoparticles, *J. Phys. Chem. C* **124**, 15665 (2020).
- [8] F. Baletto, Structural properties of sub-nanometer metallic clusters, *J. Phys.: Condens. Matter* **31**, 113001 (2019).
- [9] A. Andres-Arroyo, B. Gupta, F. Wang, J. J. Gooding, and P. J. Reece, Optical manipulation and spectroscopy of silicon nanoparticles exhibiting dielectric resonances, *Nano Lett.* **16**, 1903 (2016).
- [10] R. Ruger, E. van Lenthe, T. Heine, and L. Visscher, Tight-binding approximations to time-dependent density functional theory—a fast approach for the calculation of electronically excited states, *J. Chem. Phys.* **144**, 184103 (2016).
- [11] M. de Wergifosse, J. Seibert, and S. Grimme, Simplified time-dependent density functional theory (sTD-DFT) for molecular optical rotation, *J. Chem. Phys.* **153**, 084116 (2020).
- [12] E. Prodan, C. Radloff, N. J. Halas, and P. Nordlander, A hybridization model for the plasmon response of complex nanostructures, *Science* **302**, 419 (2003).
- [13] P. Nordlander, C. Oubre, E. Prodan, K. Li, and M. I. Stockman, Plasmon hybridization in nanoparticle dimers, *Nano Lett.* **4**, 899 (2004).
- [14] S. M. Morton, D. W. Silverstein, and L. Jensen, Theoretical studies of plasmonics using electronic structure methods, *Chem. Rev.* **111**, 3962 (2011).
- [15] K. L. Kelly, E. Coronado, L. L. Zhao, and G. C. Schatz, The optical properties of metal nanoparticles: The influence of size, shape, and dielectric environment, *J. Phys. Chem. B* **107**, 668 (2002).
- [16] R. Jin, Y. Cao, C. A. Mirkin, K. L. Kelly, G. C. Schatz, and J. G. Zheng, Photoinduced conversion of silver nanospheres to nanoprisms, *Science* **294**, 1901 (2001).
- [17] E. Hao and G. C. Schatz, Electromagnetic fields around silver nanoparticles and dimers, *J. Chem. Phys.* **120**, 357 (2004).
- [18] J. I. Fuks, L. Lacombe, S. E. B. Nielsen, and N. T. Maitra, Exploring non-adiabatic approximations to the exchange–correlation functional of TDDFT, *Phys. Chem. Chem. Phys.* **20**, 26145 (2018).
- [19] K. Jiang and M. Pavanello, Time-dependent orbital-free density functional theory: Background and Pauli kernel approximations, *Phys. Rev. B* **103**, 245102 (2021).
- [20] A. J. White, O. Certik, Y. H. Ding, S. X. Hu, and L. A. Collins, Time-dependent orbital-free density functional theory for electronic stopping power: Comparison to the Mermin-Kohn-Sham theory at high temperatures, *Phys. Rev. B* **98**, 144302 (2018).
- [21] Y. H. Ding, A. J. White, S. X. Hu, O. Certik, and L. A. Collins, *Ab initio* Studies on the Stopping Power of Warm Dense Matter with Time-Dependent Orbital-Free Density Functional Theory, *Phys. Rev. Lett.* **121**, 145001 (2018).
- [22] A. Schild and E. K. U. Gross, Exact Single-Electron Approach to the Dynamics of Molecules in Strong Laser Fields, *Phys. Rev. Lett.* **118**, 163202 (2017).

- [23] D. Neuhauser, S. Pistinner, A. Coomar, X. Zhang, and G. Lu, Dynamic kinetic energy potential for orbital-free density functional theory, *J. Chem. Phys.* **134**, 144101 (2011).
- [24] L. H. Thomas, The calculation of atomic fields, *Math. Proc. Cambridge Philos. Soc.* **23**, 542 (1926).
- [25] E. Fermi, Un metodo statistico per la determinazione di alcune priorietà dell'atomo, *Rend. Accad. Nazionale Lincei* **6**, 32 (1927).
- [26] M. Pi, M. Barranco, J. Nemeth, C. Ngo, and E. Tomasi, Time-dependent Thomas-Fermi approach to nuclear monopole oscillations, *Phys. Lett. B* **166**, 1 (1986).
- [27] A. Domsps, P.-G. Reinhard, and E. Suraud, Time-Dependent Thomas-Fermi Approach for Electron Dynamics in Metal Clusters, *Phys. Rev. Lett.* **80**, 5520 (1998).
- [28] M. Rusek, H. Lagadec, and T. Blenski, Cluster explosion in an intense laser pulse: Thomas-Fermi model, *Phys. Rev. A* **63**, 013203 (2000).
- [29] A. Banerjee and M. K. Harbola, Hydrodynamic approach to time-dependent density functional theory; response properties of metal clusters, *J. Chem. Phys.* **113**, 5614 (2000).
- [30] D. Michta, F. Graziani, and M. Bonitz, Quantum hydrodynamics for plasmas—a Thomas-Fermi theory perspective, *Contrib. Plasma Phys.* **55**, 437 (2015).
- [31] Z. A. Moldabekov, M. Bonitz, and T. S. Ramazanov, Theoretical foundations of quantum hydrodynamics for plasmas, *Phys. Plasmas* **25**, 031903 (2018).
- [32] W. Yan, Hydrodynamic theory for quantum plasmonics: Linear-response dynamics of the inhomogeneous electron gas, *Phys. Rev. B* **91**, 115416 (2015).
- [33] D. I. Palade and V. Baran, Optical response of C60 fullerene from a time dependent Thomas Fermi approach, *J. Phys. B: At., Mol. Opt. Phys.* **48**, 185102 (2015).
- [34] X. Shao, K. Jiang, W. Mi, A. Genova, and M. Pavanello, DFTpy: An efficient and object-oriented platform for orbital-free DFT simulations, *WIREs Comput. Mol. Sci.* **11**, e1482 (2021).
- [35] H. Xiang, X. Zhang, D. Neuhauser, and G. Lu, Size-dependent plasmonic resonances from large-scale quantum simulations, *J. Phys. Chem. Lett.* **5**, 1163 (2014).
- [36] H. Xiang, M. Zhang, X. Zhang, and G. Lu, Understanding quantum plasmonics from time-dependent orbital-free density functional theory, *J. Phys. Chem. C* **120**, 14330 (2016).
- [37] H. Xiang, Z. Wang, L. Xu, X. Zhang, and G. Lu, Quantum plasmonics in nanorods: A time-dependent orbital-free density functional theory study with thousands of atoms, *J. Phys. Chem. C* **124**, 945 (2019).
- [38] C. Covington, J. Malave, and K. Varga, Coupled maxwell and time-dependent orbital-free density functional calculations, *Phys. Rev. B* **103**, 075119 (2021).
- [39] C. Huang and E. A. Carter, Nonlocal orbital-free kinetic energy density functional for semiconductors, *Phys. Rev. B* **81**, 045206 (2010).
- [40] W. Mi, A. Genova, and M. Pavanello, Nonlocal kinetic energy functionals by functional integration, *J. Chem. Phys.* **148**, 184107 (2018).
- [41] W. Mi and M. Pavanello, Orbital-free density functional theory correctly models quantum dots when asymptotics, nonlocality, and nonhomogeneity are accounted for, *Phys. Rev. B* **100**, 041105(R) (2019).
- [42] G. Vignale and W. Kohn, Current-Dependent Exchange-Correlation Potential for Dynamical Linear Response Theory, *Phys. Rev. Lett.* **77**, 2037 (1996).
- [43] G. Vignale, C. A. Ullrich, and S. Conti, Time-Dependent Density Functional Theory Beyond the Adiabatic Local Density Approximation, *Phys. Rev. Lett.* **79**, 4878 (1997).
- [44] M. E. Casida, Time-dependent density functional response theory for molecules, in *Recent Advances in Density Functional Methods* (World Scientific, 1995), pp. 155–192.
- [45] L. Dalcín, R. Paz, M. Storti, and J. D'Elía, MPI for python: Performance improvements and MPI-2 extensions, *J. Parallel Distributed Comput.* **68**, 655 (2008).
- [46] W. L. Schaich, A hydrodynamic model calculation of linear and nonlinear optical response in an asymmetric parabolic quantum well, *Solid State Commun.* **88**, 5 (1993).
- [47] K. Yabana, T. Nakatsukasa, J.-I. Iwata, and G. F. Bertsch, Real-time, real-space implementation of the linear response time-dependent density-functional theory, *Physica Status Solidi B* **243**, 1121 (2006).
- [48] C. A. Ullrich, *Time-Dependent Density-Functional Theory: Concepts and Applications* (Oxford University Press, New York, 2011).
- [49] R. van Leeuwen and E. J. Baerends, Energy expressions in density-functional theory using line integrals, *Phys. Rev. A* **51**, 170 (1995).
- [50] A. P. Gaiduk, S. K. Chulkov, and V. N. Staroverov, Reconstruction of density functionals from Kohn-Sham potentials by integration along density scaling paths, *J. Chem. Theory Comput.* **5**, 699 (2009).
- [51] A. Genova, D. Ceresoli, A. Krishtal, O. Andreussi, R. A. DiStasio, and M. Pavanello, eQE: An open-source density functional embedding theory code for the condensed phase, *Int. J. Quantum Chem.* **117**, e25401 (2017).
- [52] W. Mi, X. Shao, A. Genova, D. Ceresoli, and M. Pavanello, eQE version 2.0: Subsystem DFT beyond GGA functionals, *Comput. Phys. Commun.* **269**, 108122 (2021).
- [53] A. Krishtal, D. Ceresoli, and M. Pavanello, Subsystem real-time time dependent density functional theory, *J. Chem. Phys.* **142**, 154116 (2015).
- [54] J. P. Perdew and A. Zunger, Self-interaction correction to density-functional approximations for many-electron systems, *Phys. Rev. B* **23**, 5048 (1981).
- [55] W. Mi, S. Zhang, Y. Wang, Y. Ma, and M. Miao, First-principle optimal local pseudopotentials construction via optimized effective potential method, *J. Chem. Phys.* **144**, 134108 (2016).
- [56] F. Alkan and C. M. Aikens, TD-DFT and TD-DFTB investigation of the optical properties and electronic structure of silver nanorods and nanorod dimers, *J. Phys. Chem. C* **122**, 23639 (2018).
- [57] H. E. Johnson and C. M. Aikens, Electronic structure and TDDFT optical absorption spectra of silver nanorods, *J. Phys. Chem. A* **113**, 4445 (2009).
- [58] B.-J. Wang, Y. Xu, and S.-H. Ke, Plasmon excitations in sodium atomic planes: A time-dependent density functional theory study, *J. Chem. Phys.* **137**, 054101 (2012).
- [59] X. Huang, E. Lindgren, and J. R. Chelikowsky, Surface passivation method for semiconductor nanostructures, *Phys. Rev. B* **71**, 165328 (2005).
- [60] K. Luo, V. V. Karasiev, and S. B. Trickey, A simple generalized gradient approximation for the noninteracting

- kinetic energy density functional, *Phys. Rev. B* **98**, 041111(R) (2018).
- [61] U. Woggon, *Optical Properties of Semiconductor Quantum Dots* (Springer, Berlin, 1997).
- [62] X. Shao, W. Mi, and M. Pavanello, Efficient DFT solver for nanoscale simulations and beyond, *J. Phys. Chem. Lett.* **12**, 4134 (2021).
- [63] A. Mangababu, G. S. Dev, B. Chandu, M. Bharati, P. Debashish, S. V. Rao, and S. N. Rao, Fabrication and characterization of GaAs nanoparticles achieved using femtosecond laser ablation, *Mater. Today: Proc.* **33**, 2385 (2020).
- [64] H. R. Philipp and H. Ehrenreich, Optical properties of semiconductors, *Phys. Rev.* **129**, 1550 (1963).
- [65] V. V. Karasiev, D. Chakraborty, and S. B. Trickey, Progress on new approaches to old ideas: Orbital-free density functionals, in *Many-Electron Approaches in Physics, Chemistry and Mathematics* (Springer International Publishing, 2014), pp. 113–134.
- [66] S. Laricchia, E. Fabiano, L. A. Constantin, and F. Della Sala, Generalized gradient approximations of the noninteracting kinetic energy from the semiclassical atom theory: Rationalization of the accuracy of the frozen density embedding theory for nonbonded interactions, *J. Chem. Theory Comput.* **7**, 2439 (2011).
- [67] L. A. Constantin, E. Fabiano, and F. Della Sala, Semilocal PauliGaussian kinetic functionals for orbital-free density functional theory calculations of solids, *J. Phys. Chem. Lett.* **9**, 4385 (2018).
- [68] L. A. Constantin, E. Fabiano, and F. Della Sala, Performance of semilocal kinetic energy functionals for orbital-free density functional theory, *J. Chem. Theory Comput.* **15**, 3044 (2019).
- [69] S. Laricchia, L. A. Constantin, E. Fabiano, and F. Della Sala, Laplacian-level kinetic energy approximations based on the fourth-order gradient expansion: Global assessment and application to the subsystem formulation of density functional theory, *J. Chem. Theory Comput.* **10**, 164 (2014).
- [70] S. Śmiga, L. A. Constantin, F. Della Sala, and E. Fabiano, The role of the reduced Laplacian renormalization in the kinetic energy functional development, *Computation* **7**, 65 (2019).
- [71] H. M. Baghramyan, F. Della Sala, and C. Ciraci, Laplacian-level quantum hydrodynamic theory for plasmonics, *Phys. Rev. X* **11**, 011049 (2021).
- [72] F. Sarcinella, E. Fabiano, L. A. Constantin, and F. Della Sala, Nonlocal kinetic energy functionals in real space using a Yukawa-potential kernel: Properties, linear response, and model functionals, *Phys. Rev. B* **103**, 155127 (2021).
- [73] <http://oarc.rutgers.edu>.
- [74] A. Castro, M. A. L. Marques, and A. Rubio, Propagators for the time-dependent KohnSham equations, *J. Chem. Phys.* **121**, 3425 (2004).
- [75] A. Gómez Pueyo, M. A. L. Marques, A. Rubio, and A. Castro, Propagators for the time-dependent KohnSham equations: Multistep, RungeKutta, exponential RungeKutta, and commutator free magnus methods, *J. Chem. Theory Comput.* **14**, 3040 (2018).